Clays and Clay Minerals, Vol. 68, No. 1:81–88, 2020

EXTREMELY Al-DEPLETED CHLORITES FROM DOLOMITE CARBONATITES OF THE KOVDOR ULTRAMAFIC-ALKALINE COMPLEX, KOLA PENINSULA, RUSSIA

Nikita V. Chukanov[1]*, Maria G. Krzhizhanovskaya[2], Igor V. Pekov[3], Dmitry A. Varlamov[4], Konstantin V. Van[4], Vera N. Ermolaeva[4], and Svetlana A. Vozchikova[1]

[1]Institute of Problems of Chemical Physics, Russian Academy of Sciences, Chernogolovka, Moscow, Region 142432, Russia
[2]Department of Crystallography, Saint Petersburg State University, Universitetskaya Nab. 7/9, 199034 St. Petersburg, Russia
[3]Faculty of Geology, Moscow State University, Vorobievy Gory, Moscow 119234, Russia
[4]Institute of Experimental Mineralogy, Russian Academy of Sciences, Chernogolovka, Moscow, Region 142432, Russia

Abstract—The problem to be solved is whether Al is a necessary component of Fe-Mg chlorites. Very unusual Al-depleted and Fe-enriched trioctahedral chlorites with the empirical formulae $Na_{0.05}Ca_{0.05}(Fe^{2+}_{3.01}Mg_{2.01}Ti_{0.14}Fe^{3+}_{0.04})_{\Sigma 6.00}[(Si_{3.53}Fe^{3+}_{0.41}Al_{0.06})_{\Sigma 4.00}O_{10}](OH)_8{\cdot}nH_2O$ (Sample 1) and $Na0.05Ca_{0.01}(Fe^{2+}_{3.26}Mg_{1.97}Fe^{3+}_{0.75}Mn_{0.01}Ti_{0.01})_{\Sigma 6.00}[(Si_{3.16}Fe^{3+}_{0.75}Al_{0.09})_{\Sigma 4.00}O_{10}](OH)_8$ (Sample 2) have been discovered in Al-depleted dolomite carbonatites of the Kovdor complex of ultramafic, alkaline rocks and carbonatites, Kola Peninsula, Russia. The presence of substantial amounts of Ti in Sample 1 is another unusual feature of this mineral. In both samples, chlorites are intimately intergrown with cronstedtite-1*T* which is an indication of a low stability of chlorite structure in the absence of aluminum in the tetrahedral sheet. The crystal structure of chlorite in Sample 1 was solved by the Rietveld method. The mineral is triclinic (IIb-4-module), space group *C*-1, $a = 5.4153(4)$, $b = 9.3805(7)$, $c = 14.5743(12)$ Å, $\alpha = 90.137(5)°$, $\beta = 96.928(5)°$, $\gamma = 90.043(6)°$, $V = 734.95(10)$ Å^3, and $Z = 2$. A problem to be solved is how stable are Al-free chlorites belonging to the clinochlore–chamosite solid-solution series and whether their existence in natural mineral assemblages is possible. The results obtained indicate that even though Al-depleted chlorites belonging to the clinochlore–chamosite solid-solution series exist in Nature as metastable phases, these minerals are extremely rare and much less stable than Al-poor serpentines.

Keywords—Chlorite · Cronstedtite · Crystal structure · Dolomite carbonatite · Infrared spectroscopy · Kovdor Complex · Rietveld refinement

INTRODUCTION

Mg-Fe-Al-chlorites, which are members of the clinochlore–chamosite solid-solution series, with the simplified general formula $(Mg,Fe,Al,\square)_6(Si,Al)_4O_{10}(OH)_8$, are characterized by wide compositional variations and polytypism, II*b*-2*n* being the most common kind of trioctahedral chlorite module (Durovic et al. 1983; Bailey 1988; Chukhrov 1992). The Al_2O_3 content typically varies in the range from ~12 wt.% in chamosite $(Fe,Al,Mg)_6(Si,Al)_4O_{10}(OH)_8$ to ~52 wt.% in donbassite, ideally $Al_{4.33}(Si_3Al)O_{10}(OH)_8$ (Hey 1954; Bondi et al. 1976; Shikazono & Kawahata 1987; Bailey 1988; Bailey & Lister 1989; Hillier & Velde 1991; Prieto et al. 1991; Zane & Sassi 1998; López-Munguira et al. 2002; Deer et al. 2009; Tang et al. 2017; Bobos et al. 2018; Wu et al. 2019). Smaller Al_2O_3 contents (down to 4 wt.%) have been found in some varieties of so-called "hydroferrichlorites," which are insufficiently investigated components of sedimentary iron ores of the Kerch iron-ore basin where chlorites are intimately intergrown with other minerals including smectites and mixed-layered phyllosilicates (Strakhov 1966; Chukhrov 1992).

Unlike trioctahedral chlorites, Al-free trioctahedral serpentines, including those with Fe^{3+} having tetrahedral coordination [cronstedtite $Fe^{2+}_2Fe^{3+}(SiFe^{3+})O_5(OH)_4$ (Hybler 2014, 2016; Hybler et al. 2016, 2017; Pignatelli et al. 2018) and guidottite $Mn^{2+}_2Fe^{3+}(SiFe^{3+})O_5(OH)_4$ (Wahle et al. 2010)] are common in Nature. This fact may be an indication of the important role of aluminum at the tetrahedral sites in the stabilization of the chlorite-type structure. Recent data, however, indicated the existence of exceptions from this general trend.

The purpose of this study was to characterize the very unusual trioctahedral Fe-rich chlorites containing no more than ~0.7 wt.% Al_2O_3 (i.e. <0.1 Al atoms per formula unit = apfu) from dolomite carbonatites of the Kovdor ultramafic-alkaline complex, Kola Peninsula, Russia, to understand better the anomalously large Ti content of these minerals. In the current nomenclature of Fe-Mg chlorites (unlike the nomenclature schemes of micas and some other phyllosilicates), the population of separate octahedral and tetrahedral sites is not taken into account. For this reason minerals described here were considered to be Al-depleted varieties of chamosite, the general formula of which is $(Fe,Al,Mg)_6(Si,Al)_4O_{10}(OH)_8$ (Back 2018; see IMA list of minerals https://www.ima-mineralogy.org/Minlist.htm - http://cnmnc.main.jp/IMA_Master_List_(2020-01).pdf).

* E-mail address of corresponding author: chukanov@icp.ac.ru
DOI: 10.1007/s42860-019-00055-8

Electronic supplementary material The online version of this article (https://doi.org/10.1007/s42860-019-00055-8) contains supplementary material, which is available to authorized users.

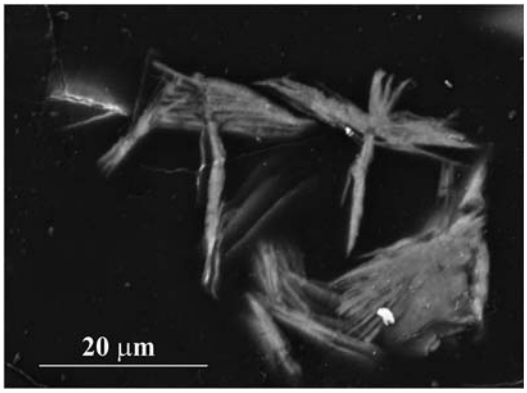

Fig. 1 Aggregates of chlorite (Sample 1) from dolomite carbonatite of the Kovdor complex. Back-scattered electron BSE image.

EXPERIMENTAL

Materials

The chlorite samples investigated in this work originated from dolomite carbonatite veins uncovered by open pit working at the Zheleznyi (Iron) Mine situated in the western part of the Kovdor complex of ultramafic, alkaline rocks, and carbonatites. The Kovdor complex is a central-type multiphase intrusion (with prevailing olivinites in the central part and alkaline rocks in peripheral zones) emplaced into Archean gneisses. Dolomite carbonatites form veins up to 2 m thick which are confined to a concentric zoned stock of phoscorites and magnetite-carbonate rocks which form the so-called Kovdor Iron-Ore Complex (Ivanyuk et al. 2002).

Two chlorite samples were investigated. In Sample 1, chlorite forms compact crusts (up to 0.2 mm thick) and rare aggregates (up to 30 μm across) of thin lamellae (Fig. 1).

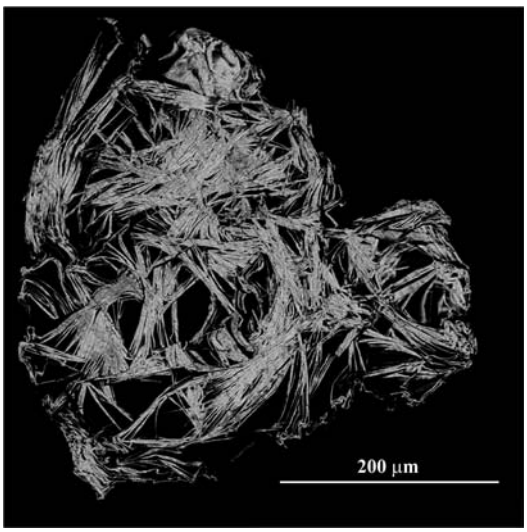

Fig. 2 Aggregates of chlorite (Sample 2) from dolomite carbonatite of the Kovdor complex. BSE image.

The associated minerals are dolomite, ilmenite, anatase, sphalerite, pyrite, hydroxycalciopyrochlore, and labuntsovite-Mg. In Sample 2, chlorite forms aggregates (up to 0.3 mm across) consisting of thin lamellae (up to 10 μm×200 μm×200 μm, see Fig. 2) in association with dolomite and labuntsovite-Mg. In both assemblages chlorites are the latest minerals to have formed.

Methods

Chemical data were obtained on polished samples embedded in epoxy resin using a Tescan VEGA-II XMU INCA Energy 450 (Tescan Orsay Holding, Brno, Czech Republic, https://www.tescan.com) microprobe instrument (EDS mode, 20 kV, 190 pA, 180 nm beam diameter, excitation zone of 3–4 μm) housed in the Institute of Experimental Mineralogy RAS, Chernogolovka, Russia. Five spot analyses were carried out for each sample. The following standards were used: MgF_2 for F, MgO for Mg, wollastonite for Ca, albite for Na, synthetic Al_2O_3 for Al, orthoclase for K, quartz for Si, and pure Mn, Fe, and Ti for these corresponding elements. Contents of other components were below detection limits of electron microprobe analysis. H_2O could not be determined because of insufficient amounts of monomineral fractions. The presence of OH groups was confirmed by means of infrared (IR) spectroscopy.

In order to obtain IR absorption spectra, powdered samples were mixed with anhydrous KBr (with the KBr to sample ratio of 200:1), pelletized, and analyzed using an ALPHA FTIR spectrometer (Bruker Optics, Karlsruhe, Germany) housed in the Institute of Problems of Chemical Physics RAS, Chernogolovka, Russia. The measurements were carried out at a resolution of 4 cm^{-1} and 16 scans per sample. The IR spectrum of an analogous pellet of pure KBr was used as a reference.

Powder X-ray diffraction data of both samples were collected at St Petersburg State University, with a Rigaku R-AXIS Rapid II diffractometer equipped with a cylindrical image plate detector (radius 127.4 mm) using Debye-Scherrer geometry, CoKα radiation (rotating anode with VariMAX microfocus optics), 40 kV, 15 mA, and an exposure time of 10 min. Data were integrated using the software package *Osc2Tab* (Britvin et al. 2017).

The unit-cell and the full-profile refinement of the XRD patterns were performed with the program package *Topas 5* (Bruker AXS 2014). The details of the structure refinement by the Rietveld method using data for clinochlore-IIb-4 from Zanazzi *et al*. (2009) as a starting model are shown in Table 1.

RESULTS

Chemical Composition

Analytical data are given in Table 2. Additionally, IR spectra (see below) revealed the presence of trace amounts of H_2O molecules in Sample 1 and the absence of H_2O in Sample 2. The empirical formulae calculated on the basis of $O_{10}(OH)_8$

https://doi.org/10.1007/s42860-019-00055-8 Published online by Cambridge University Press

and 10 Mg+Mn+Fe+Al+Ti+Si apfu, taking into account the charge-balance requirement are:

$Na_{0.05}Ca_{0.05}(Fe^{2+}{}_{3.01}Mg_{2.01}Ti_{0.14}Fe^{3+}{}_{0.04})_{\Sigma 6.00}[(Si_{3.53}Fe3+_{0.41}Al_{0.06})_{\Sigma 4.00}O_{10}](OH)_8 \cdot nH_2O$ (Sample 1);

$Na_{0.05}Ca_{0.01}(Fe^{2+}{}_{3.26}Mg_{1.97}Fe^{3+}{}_{0.75}Mn_{0.01}Ti_{0.01})_{\Sigma 6.00}[(Si_{3.16}Fe^{3+}{}_{0.75}Al_{0.09})_{\Sigma 4.00}O_{10}](OH)_8$ (Sample 2).

Infrared Spectroscopy

IR spectra of the Al-deficient chlorite Samples 1 and 2 (Fig. 3) were similar. The strongest bands were observed in the ranges 3300–3700 cm^{-1} (O–H stretching vibrations), 950–1050 cm^{-1} (stretching vibrations of the tetrahedral sheet), 640–650 cm^{-1} (O–Si–O bending vibrations), and 400–500 cm^{-1} (lattice modes involving Si–O–Si bending and (Fe,Mg)–O stretching vibrations). Additional weak bands at 1640 and 561 cm^{-1} in the IR spectrum of sample 1 were due to H–O–H bending and libration vibrations of trace amounts of H_2O molecules, respectively.

Bands of O–H stretching vibrations in the IR spectrum of Sample 2 were shifted toward the low-frequency region relative to analogous bands in the IR spectrum of Sample 1. The lowering of the former may be due to a rather strong polarization of OH groups coordinated by Fe^{3+} and, as a result, stronger hydrogen bonds formed by $Fe^{3+}(Mg,Fe^{2+})_2O$–H groups as compared with $(Mg,Fe^{2+})_3O$–H groups. Shifts in these bands towards lower frequencies with the enhancement of the ^{VI}Fe content was a general trend for trioctahedral chlorites (Prieto et al. 1991).

According to Libowitzky (1999), the correlation between the O···O distance $d_{O\cdots O}$ (i.e. the distance between O atoms of the OH group and H-bond acceptor, in Å) and wavenumber ν_{OH} (in cm^{-1}) of a band of O–H stretching vibrations is described by the equation $d_{O\cdots O} = 0.1321[26.44–\ln(3592–\nu_{OH})]$. The $d_{O\cdots O}$ distances estimated using this equation were 2.726 and 3.118 Å for Sample 1, and 2.809 and >3.23 Å for Sample 2.

The band of stretching vibrations of the tetrahedral sheet in the IR spectrum of Sample 1 was observed at 960 cm^{-1} whereas an analogous band of Sample 2 had an absorption maximum at a smaller wavenumber value of 953 cm^{-1}. This agrees with the general trend for silicates, according to which weighted average frequency of $^{[4]}(Si,Al,Fe^{3+})$–O stretching vibrations decreases as the fraction of trivalent species among cations with octahedral coordination increases (Chukanov 2014).

X-ray Diffraction Data and Crystal Structure

Powder XRD patterns of the Samples 1 and 2 (Fig. 4, Table 3) were similar and corresponded to IIb-4-module trioctahedral chlorites with cronstedtite-1*T* impurities (~10 and 30%, respectively; see Hybler 2014, 2016; Hybler et al. 2016, 2017; Pignatelli et al. 2018). Parameters of the triclinic unit cell for Sample 1 are given in Table 1. Unit-cell parameters of Sample 2 calculated based on the same model were: $a = 5.42(1)$, $b = 9.41(2)$, $c = 14.55(4)$ Å, $\alpha = 90.02(4)$, $\beta = 97.05(7)$, $\gamma = 90.04(4)°$, and $V = 736(1)$ $Å^3$.

Table 1. Structure refinement details and crystallographic data for Sample 1.

Starting model	Clinochlore (IIb-4) (Zanazzi et al. 2009)
Crystal system	Triclinic
Space group, *Z*	*C*-1, 2
a (Å)	5.4153(4)
b (Å)	9.3805(7)
c (Å)	14.5743(12)
α (deg.)	90.137 (5)
β (deg.)	96.928 (5)
γ (deg.)	90.043 (6)
V ($Å^3$)	734.95(10)
D_X (g/cm^3)	2.8895(4)
Radiation type	$CoK\alpha_{1+2}$
2θ range (degrees)	5–140
Number of reflections	900
R_p %	1.67
R_{wp} %	2.45
R_{exp} %	0.66
R_B %	1.33
GOF	3.69
Impurity	Cronstedtite-1*T*
wt. %	10.2(1)

Rietveld refinement for Sample 2 could not be carried out correctly because of a pronounced texture. Structural data were obtained, therefore, only for the chlorite component in Sample 1. The final Rietveld plot is shown in Fig. 1S.

Table 2. Chemical composition of Al-deficient chlorites (wt.%).

Constituent	Sample 1		Sample 2	
	Mean	Range	Mean	Range
Na_2O	0.22	*bdl*–0.34	0.21	*bdl*–0.48
CaO	0.40	0.18–0.56	0.08	*bdl*–0.25
MgO	17.06	16.43–17.81	11.60	10.90–12.29
MnO	*bdl*	*bdl*	0.08	bdl–0.21
FeO	32.57	36.44–39.87*	34.13	47.60–50.81*
Fe_2O_3	5.41		17.45	
Al_2O_3	0.49	*bdl*–0.72	0.64	0.48–0.85
TiO_2	1.73	1.30–2.10	0.13	bdl–0.31
SiO_2	31.81	30.21–33.18	27.66	26.86–28.53
Total	89.69		91.98	

bdl = below detection limit.

*The ranges are given for total Fe contents calculated as FeO which was apportioned between FeO and Fe_2O_3 based on the charge-balance requirement for the empirical formulae calculated on the basis of $O_{10}(OH)_8$ and 10 Mg+Mn+Fe+Al+Ti+Si apfu.

https://doi.org/10.1007/s42860-019-00055-8 Published online by Cambridge University Press

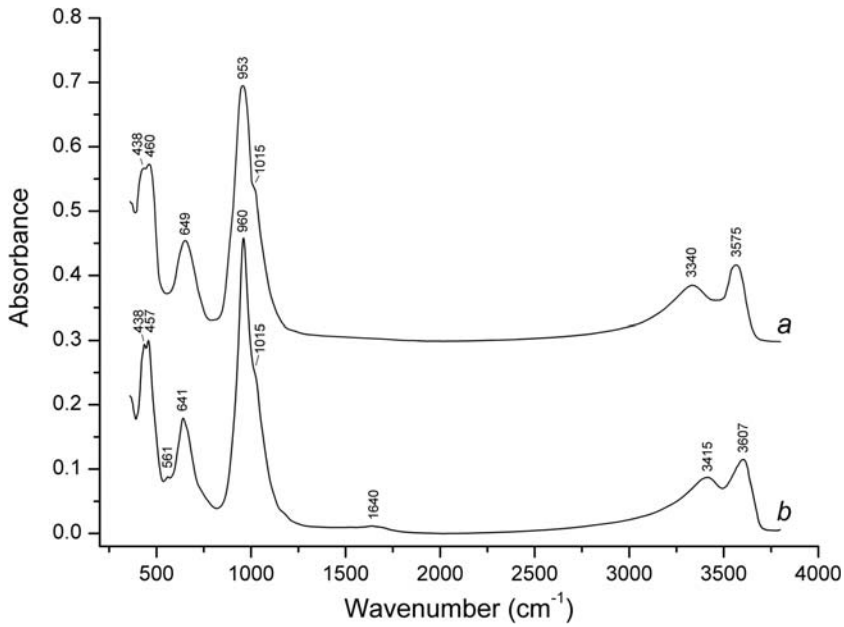

Fig. 3 Infrared absorption spectra of **a** Sample 2 and **b** Sample 1.

Atomic coordinates were refined for all sites except *M*1 and *M*4, which are special positions (Table 4). Isotropic displacement parameters B_{iso} were used for all the atoms; B_{iso} were constrained for the groups of atoms (Si1–Si2, *M*1–*M*4, and O1–O9). The restraints for the Si–O bonds and O–Si–O angles in tetrahedra, as well as selected distances in $(Fe,Mg)O_6$ octahedra, were realized using *Topas 5 Launch* mode with the weighting factor for penalties $K = 3$. A polyhedral image of the crystal structure of Al-deficient chlorite (Sample 1) is given in Fig. 5. Selected bond lengths are listed in Table 5.

Variations in bond lengths in tetrahedra ranged from 1.59 to 1.67 Å, with average values of 1.625 Å for $Si1O_4$ and 1.63 Å for $Si2O_4$, which are slightly longer than the typical value for chlorites of 1.62 Å (Liebau 1985) and may be due to the Fe^{3+} admixture at the tetrahedral sites. The angles O–Si1–O and O–Si2–O varied in the ranges 102.9–115.9° and 100.8–115.1°, respectively.

In the structure of the chlorite component in Sample 1, iron concentrated in the *M*1 and *M*2 sites belonging to the *TOT* triple block whereas *M*3 and *M*4 sites of the simple octahedral layer were Mg-dominant (Table 4) and, correspondingly, were characterized by shorter *M*–O distances (Table 5). The chlorites under study have the largest unit-cell volumes of any chlorites presented in the ICSD database (2017), which is apparently due to the large total Fe content and the presence of significant amounts of Fe^{3+} in the tetrahedral sites.

DISCUSSION

The formation of Al-depleted chlorites in dolomite carbonatites is associated with a small total Al content in

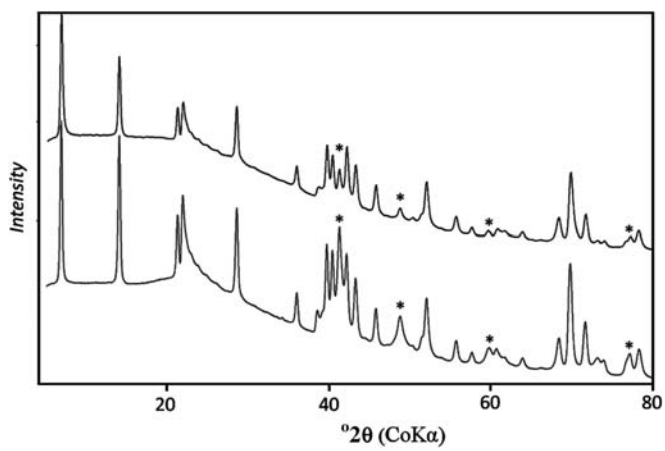

Fig. 4 Powder X-ray diffraction patterns of Sample 1 (upper trace) and Sample 2 (lower trace). Diagnostic peaks of the cronstedtite-1*T* admixture are indicated with asterisks.

https://doi.org/10.1007/s42860-019-00055-8 Published online by Cambridge University Press

Table 3. Powder X-ray diffraction data of Al-depleted chlorites from Kovdor.

Sample 2		Sample 1				*hkl*
I_{obs}	d_{obs}, Å	I_{obs}	d_{obs}, Å	I_{calc}*	d_{calc}, Å	
100	14.46	100	14.40	100	14.47	001
89	7.22	59	7.21	64	7.234	002
32	4.815	21	4.810	17	4.823	003
44	4.677	25	4.664	3, 9, 12	4.690, 4.666, 4.663	020, 1-10, 110
		11	4.580	2, 7	4.582, 4.581	1-1-1, 11-1
11	4.477	5	4.462	19, 6	4.465, 4.458	0-21
5	4.311	2	4.306	3, 1	4.313, 4.306	1-11, 111
1	3.945	1	3.932	5	3.931	022
45	3.611	35	3.608	31	3.617	004
12	2.889	11	2.887	11	2.894	005
8	2.706	5	2.691	2, 2, 1, 2	2.702, 2.702, 2.687, 2.686	20-1, 130, 1-3-1, 13-1
38	2.630	28	2.625	18, 13	2.626, 2.625	131, 20-2
35	2.587	23	2.583	8, 12, 1, 7	2.587, 2.585, 2.584, 2.583	201, 13-2, 11-5, 1-3-2
33	2.485	29	2.480	21, 18, 19	2.486, 2.480, 2.478	1-32, 132, 20-3
22	2.424	19	2.421	15, 13, 12	2.426, 2.423, 2.420	202, 13-3, 1-3-3
12	2.298	12	2.295	9, 8, 10	2.302, 2.296, 2.294	1-33, 133, 20-4
19	2.039	17	2.037	15, 15, 13	2.043, 2.040, 2.036	204, 13-5, 1-3-5
6	1.915	5	1.914	5, 5	1.916, 1.913	135, 20-6
4	1.772	3	1.767	2	1.767	1-5-1
2	1.692	2	1.690	2	1.691	1-3-7
9	1.593	8	1.592	4, 6	1.594, 1.592	137, 20-8
38	1.565	27	1.562	12, 11, 12	1.564, 1.563, 1.563	3-3-1, 060, 33-1
14	1.530	10	1.527	2, 2, 2, 2, 3, 3	1.530, 1.529, 1.528, 1.527, 1.527, 1.527	3-31, 0-62, 331, 062, 3-3-3, 33-3
3	1.444	2	1.443	4	1.447	0.0.10
6	1.437	4	1.434	1, 1, 1	1.435, 1.434, 1.433	333, 064, 3-3-5
7	1.419	6	1.418	3, 4	1.421, 1.419	13-9, 1-3-9

*For the calculated pattern, only reflections with intensities ≥1% are given.

Reflections belonging to cronstedtite are not included.

these rocks. Other minor (non-carbonate) minerals of the Kovdor dolomite carbonatites are represented predominantly by Al-free amphiboles (mainly, richterite), Al-free serpentines, Al-deficient trioctahedral micas (namely $^{IV}Fe^{3+}$-bearing phlogopite $KMg_3[Si_3(Al,Fe^{3+})O_{10}](OH)_2$ and tetraferriphlogopite $KMg_3[Si_3Fe^{3+}O_{10}](OH)_2$), magnetite, zircon, minerals from the labuntsovite-Mg-labuntsovite-Fe series $Na_4K_4(Mg,Fe^{2+})_2(Ti,Nb)_8(Si_4O_{12})_4(OH,O)_8 \cdot 10H_2O$, Al-free phosphates, pyrrhotite, and pyrite. Consequently, even phlogopite, which is the main concentrator of Al in these rocks, is Al-depleted because of the large Fe^{3+} content.

Both chamosite samples investigated in this work contain admixed cronstedtite-1*T*. This fact, along with the extreme rarity in Nature of Al-depleted chlorites with Al_2O_3 contents of <1 wt.% (unlike Al-depleted serpentines), is an indirect indication of a small area of thermodynamic stability of Al-free chlorites compared to Al-bearing chlorites. The data above, however, show that the existence of Al-depleted trioctahedral chlorites is a reliably established fact.

The presence of significant amounts of Ti is not typical of chlorites. The largest TiO_2 contents (up to 1.2 wt.%) have been detected in Fe-rich chlorites: chamosite from gabbro of the Pechenga region, Kola Peninsula (Chukhrov 1992), and Al-poor chamosite (with 14.64 wt.% Al_2O_3) forming pseudomorphs after biotite from granite of the Monzoni intrusive complex, Italy (Bondi et al. 1976). The relatively large amount of Ti in Sample 1 (locally, up to ~2 wt.% TiO_2) confirms this tendency. On the basis of the available data, drawing an unambiguous conclusion as to whether this tendency has a crystal chemical or a genetic origin is impossible. Another problem to be solved (maybe, based on experimental data from synthesis) is how stable are Al-free chlorites belonging to the clinochlore–chamosite solid-solution series and whether their transformation into serpentines is possible.

https://doi.org/10.1007/s42860-019-00055-8 Published online by Cambridge University Press

Table 4. The atomic coordinates, site occupation, and isotropic displacement parameters (Å^2) of chlorite in Sample 1.

Site	Wyckoff symbol	*x/a*	*y/b*	*z/c*	Atom	Occupation	B_{iso} (Å^2)
Si1	4i	0.248(2)	0.166(1)	0.1972(8)	Si	1	1.09(9)
Si2	4i	0.735(2)	0.009(1)	0.1955(7)	Si	1	1.09(9)
*M*1	2a	0	0	0	Mg	0.18	1.68(7)
					Fe	0.82	
*M*2	4i	–0.010(2)	0.325(1)	0	Mg	0.26	1.68(7)
					Fe	0.74	
*M*3	4i	–0.009(2)	0.178(2)	0.5	Mg	0.67	1.68(7)
					Fe	0.33	
*M*4	2h	0	0.5	0.5	Mg	1	1.68(7)
O1	4i	0.232(3)	0.154(2)	0.088(1)	O	1	1.1(1)
O2	4i	0.686(4)	–0.003(3)	0.085(2)	O	1	1.1(1)
O3	4i	0.225(4)	0.337(2)	0.225(1)	O	1	1.1(1)
O4	4i	0.508(4)	0.091(2)	0.232(1)	O	1	1.1(1)
O5	4i	0.014(4)	0.075(2)	0.232(1)	O	1	1.1(1)
O6	4i	0.701(4)	0.342(2)	0.091(2)	O	1	1.1(1)
O7	4i	0.145(4)	0.016(3)	0.435(1)	O	1	1.1(1)
O8	4i	0.156(3)	0.341(3)	0.423(2)	O	1	1.1(1)
O9	4i	0.635(3)	0.162(2)	0.405(1)	O	1	1.1(1)

The presence of pyrite in Sample 1 indicates reducing conditions in which this mineral association was formed. This, along with a deficiency of aluminum, may have caused Ti, rather than Fe^{3+}, to be the main charge-balancing, high-valence octahedral cation.

SUMMARY

Results obtained during the present study confirmed the existence of extremely Al-depleted trioctahedral chlorites (with Al_2O_3 contents of <10 wt.% and, in particular, <1 wt.%) in

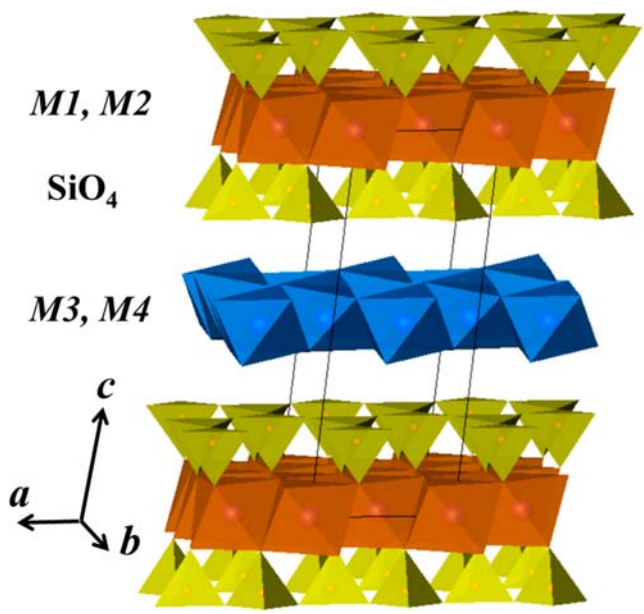

Fig. 5 General view of the crystal structure of Al-deficient chlorite (Sample 1). The unit cell is outlined. The *M*1 and *M*2 sites are Fe^{2+}-dominant, and the *M*3 and *M*4 sites are enriched in Mg.

https://doi.org/10.1007/s42860-019-00055-8 Published online by Cambridge University Press

Table 5. Selected bond lengths (Å) in Al-deficient chlorite (Sample 1).

Bond	Bond length (Å)	Bond	Bond length (Å)
Si1–O1	1.59(2)	Si2–O4	1.59(2)
–O4	1.60(2)	–O2	1.61(3)
–O5	1.65(2)	–O5	1.66(2)
–O3	1.66(2)	–O3	1.67(2)
<Si1–O>	1.625	<Si2–O>	1.63
*M*1–O6×2	2.19(2)	*M*3–O7	2.02(2)
–O1×4	2.22(2)	–O8	2.10(2)
<*M*1–O>	2.210	–O8'	2.15(2)
*M*2–O1	2.10(2)	–O9	2.20(2)
–O6	2.18(2)	–O7	2.22(2)
–O2	2.21(2)	–O9'	2.24(2)
–O6'	2.22(2)	<*M*3–O>	2.155
–O2'	2.23(2)	*M*4–O7×2	2.04(2)
–O1'	2.35(2)	–O8×2	2.10(2)
<*M*2–O>	2.215	–O9 ×2	2.23(2)
		<*M*4–O>	2.12

Nature, as well as the possibility of the occurrence of significant amounts of Fe^{3+} and Ti in the tetrahedral and octahedral sites, respectively, of these minerals. The extreme rarity of Al-depleted chlorites (unlike Al-depleted serpentines) and the presence of cronstedtite intimately associated with such chlorites at Kovdor suggest that the structure of Al-poor chlorite may be unstable and can easily transform into the serpentine structure.

Specific conditions for mineral formation in the dolomite carbonatites of Kovdor, including a deficit of Al and reducing conditions during mineral formation, contributed to the formation of Al-poor chlorites in which Fe^{3+} rather than Al is the major trivalent cation in the tetrahedral sheet and Ti may be the major high-valency octahedral cation.

ACKNOWLEDGMENTS

This work was performed in accordance with the state task, state registration No. 0089-2019-0013. The authors thank the X-ray Diffraction Centre of Saint-Petersburg State University for instrumental and computational resources.

Compliance with ethical standards

Conflict of interest

On behalf of all authors, the corresponding author states that there is no conflict of interest.

REFERENCES

Back, M. E. (2018). *Fleischer's Glossary of Mineral Species*. Tucson, Arizona, USA: The Mineralogical Record Inc..

Bailey, S.W. (1988). Chlorites: Structures and crystal chemistry. Pp. 347–403 in: *Hydrous Phyllosilicates (Exclusive of Micas)* (S.W. Bailey, editor). Reviews in Mineralogy, **19**. Mineralogical Society of America, Chantilly, Virginia, USA.

Bailey, S. W., & Lister, J. (1989). Structures, compositions, and X-ray diffraction identification of dioctahedral chlorites. *Clays and Clay Minerals, 37*, 193–202.

Bobos, I., Noronha, F., & Mateus, A. (2018). Fe-, Fe,Mn- and Fe,Mg-chlorite: A genetic linkage to W, (Cu,Mo) mineralization in the magmatic-hydrothermal system of Borralha, northern Portugal. *Mineralogical Magazine, 82*, S259–S279.

Bondi, M., Morten, L., & Rossi, P. L. (1976). Chlorites from Italian granitoid rocks. *Tschermaks Mineralogische und Petrographische Mitteilungen, 23*, 39–50.

Britvin, S. N., Dolivo-Dobrovolsky, D. V., & Krzhizhanovskaya, M. G. (2017). Software for processing the X-ray powder diffraction data obtained from the curved image plate detector of Rigaku RAXIS Rapid II diffractometer. *Zapiski Rossiiskogo Mineralogicheskogo Obshchestva, 146*, 104–107 (in Russian).

Bruker AXS. (2014) *Topas 5.0. General profile and structure analysis software for powder diffraction data*. Karlsruhe, Germany.

Chukanov, N. V. (2014). *Infrared Spectra of Mineral Species: Extended Library*. Dordrecht–Heidelberg–New York–London: Springer-Verlag GmbH.

Chukhrov, F. V. (Ed.). (1992). *Minerals*. Moscow: Nauka (in Russian).

Deer, W. A., Howie, R. A., & Zussman, J. (2009). *Rock-forming Minerals. Layered Silicates Excluding Micas and Clay Minerals* (313 pp). London: The Geological Society.

Durovic, S., Dornberger-Schiff, K., & Weiss, Z. (1983). Chlorite polytypism. I. OD interpretation and polytype symbolism of chlorite structures. *Acta Crystallographica, B39*, 547–552.

Hey, M. H. (1954). A new review of chlorites. *Mineralogical Magazine, 30*, 277–292.

Hillier, S., & Velde, B. (1991). Octahedral occupancy and the chemical composition of diagenetic (low-temperature) chlorite. *Clay Minerals, 26*, 149–168.

Hybler, J. (2014). Refinement of cronstedtite-1M. *Acta Crystallograpica, B70*, 963–972.

Hybler, J. (2016). Crystal structure of cronstedtite-$6T_2$, a non-MDO polytype. *European Journal of Mineralogy, 28*, 777–788.

Hybler, J., Sejkora, J., & Venclík, V. (2016). Polytypism of cronstedtite from Pohled, Czech Republic. *European Journal of Mineralogy, 28*, 765–775.

Hybler, J., Števko, M., & Sejkora, J. (2017). Polytypism of cronstedtite from Nižná Slaná, Slovakia. *European Journal of Mineralogy, 29*, 91–99.

Ivanyuk, G. Y., Yakovenchuk, V. N., & Pakhomovsky, Y. A. (2002). *Kovdor* (322 pp). Apatity, Russia: Laplandia minerals.

Libowitzky, E. (1999). Correlation of O–H stretching frequencies and O–H···O hydrogen bond lengths in minerals. *Monatshefte für Chemie, 130*, 1047–1059.

Liebau, F. (1985). *Structural Chemistry of Silicates* (354 pp). Berlin–Heidelberg: Springer-Verlag.

López-Munguira, A., Nieto, F., & Morata, D. (2002). Chlorite composition and geothermometry: a comparative HRTEM/AEM-EMPA-XRD study of Cambrian basic lavas from the Ossa Morena Zone, SW Spain. *Clay Minerals, 37*, 267–281.

Pignatelli, I., Mugnaioli, E., & Marrocchi, Y. (2018). Cronstedtite polytypes in the Paris meteorite. *European Journal of Mineralogy, 30*, 349–354.

Prieto, A. C., Dubessy, A. C., & Cathelineau, M. (1991). Structure–composition relationships in trioctahedral chlorites: A vibrational spectroscopy study. *Clays and Clay Minerals, 39*, 531–539.

Shikazono, N., & Kawahata, H. (1987). Compositional differences in chlorite from hydrothermally altered rocks and hydrothermal ore deposits. *The Canadian Mineralogist, 25*, 465–474.

Strakhov, N. M. (Ed.). (1966). *Kerch Iron-ore Basin*. Moscow: Nedra 576 pp. (in Russian).

Tang, D., Shi, X., Jiang, G., Zhou, X., & Shi, Q. (2017). Ferruginous seawater facilitates the transformation of glauconite to chamosite:

An example from the Mesoproterozoic Xiamaling formation of North China. *American Mineralogist, 102*, 2317–2332.

Wahle, M. W., Bujnowski, T. J., Guggenheim, S., & Kogure, T. (2010). Guidottiite, the Mn-analogue of cronstedtite: A new serpentine group mineral from South Africa. *Clays and Clay Minerals, 58*, 364–378.

Wu, D., Pan, J., Xia, F., Huang, G., & Lai, J. (2019). The mineral chemistry of chlorites and its relationship with uranium mineralization from huangsha uranium mining area in the middle Nanling Range, SE China. *Minerals, 9*, 199, 23 pp. https://doi.org/10.3390/min9030199.

Zanazzi, P. F., Comodi, P., Nazzareni, S., & Andreozzi, G. B. (2009). Thermal behaviour of chlorite: an in-situ single-crystal and powder diffraction study. *European Journal of Mineralogy, 21*, 581–589.

Zane, A., & Sassi, R. (1998). New data on metamorphic chlorite as a petrogenetic indicator mineral, with special regard to greenschist-facies rocks. *The Canadian Mineralogist, 36*, 713–726.

(*Received 31 October 2019; revised 10 December 2019; AE: Warren D. Huff*)